

Thermal fatigue life evaluation of SnAgCu solder joints in a multi-chip power module

C Barbagallo¹, G L Malgioglio², G Petrone¹ and G Cammarata¹

¹University of Catania, Department of Industrial Engineering, Viale A. Doria 6, 95125, Catania, Italy

²STMicroelectronics, IPD R&D, Stradale Primosole 50, 95121, Catania, Italy

E-mail: gpetrone@dii.unict.it

Abstract. For power devices, the reliability of thermal fatigue induced by thermal cycling has been prioritized as an important concern. The main target of this work is to apply a numerical procedure to assess the fatigue life for lead-free solder joints, that represent, in general, the weakest part of the electronic modules. Starting from a real multi-chip power module, FE-based models were built-up by considering different conditions in model implementation in order to simulate, from one hand, the worst working condition for the module and, from another one, the module standing into a climatic test room performing thermal cycles. Simulations were carried-out both in steady and transient conditions in order to estimate the module thermal maps, the stress-strain distributions, the effective plastic strain distributions and finally to assess the number of cycles to failure of the constitutive solder layers.

1. Introduction

Recently, various electrified vehicles are emerging. Power (inverter/converter) modules, based on IGBTs and diodes, are one of the core components for such vehicles and convert battery or fuel-cell power to drive motors. Power modules equipped in electrified vehicles often operate at harsh conditions. Thermal stress is known to be one of the major factors resulting performance degradations or damages in solder joints in power modules [1]. For that reason, demand of high power density electronic converters calls for numerical methods to evaluate their reliability at the design stage. The reliability of lead-free solder joints is one of the key factors in the reliability of the overall converter, since they represent mechanical, electrical and often thermal connections between the electronic components and the board [2]. Combined with the thermal expansion mismatch between the different materials of the assembly, cyclic thermal loadings result in stress reversals and potential accumulation of inelastic strain in the solder joint. This inelastic strain accumulates with repeated cycling and ultimately causes solder joint cracking and interconnect failure [3]. Many authors [3,7,8] have studied the fatigue behaviour of lead-free solders. There is a difference between a fatigue life evaluation that uses power cycling and one that uses temperature cycling. During thermal cycling, the solder layer reaches a uniform temperature. In case of the power cycle becomes short, this state is different from the real active state of the power device, in fact the real temperature distribution on the solder layer is not uniform. [4]. The damage of solder joints, which falls in the mechanical fatigue behavior of materials, is a Low-Cycle-Fatigue (LCF) process. A characteristic of LCF is that significant plastic strains occur on the macroscopic scale during each load cycle. Because of the demand for high power density electronic converters, coupled thermo-mechanical analyses oriented to the solder joint fatigue



life prediction are becoming a topic of very high interest. In this framework, a numerical analysis on thermo-mechanical behaviour and fatigue life prediction for a power module is proposed.

2. Model implementation

Models were implemented and solved by a FE-based software devoted to multi-physical applications. In our study, we numerically analysed thermal state, thermal-induced stress-strain and we carried-out a LCF life prediction for a multi-chip power module. Model implementation and numerical solution are presented in the following paragraphs.

2.1. Geometry of the numerical model

The geometry of the studied module and the related stratigraphy are shown in Fig. 1. The module is mainly made by a copper baseplate where three power islands are arranged on. Each power island is composed by several layers, such as lead-free solders, a packed 3-layers Direct Bond Copper (DBC), the dies (IGBT and diode) equipped with front metals.

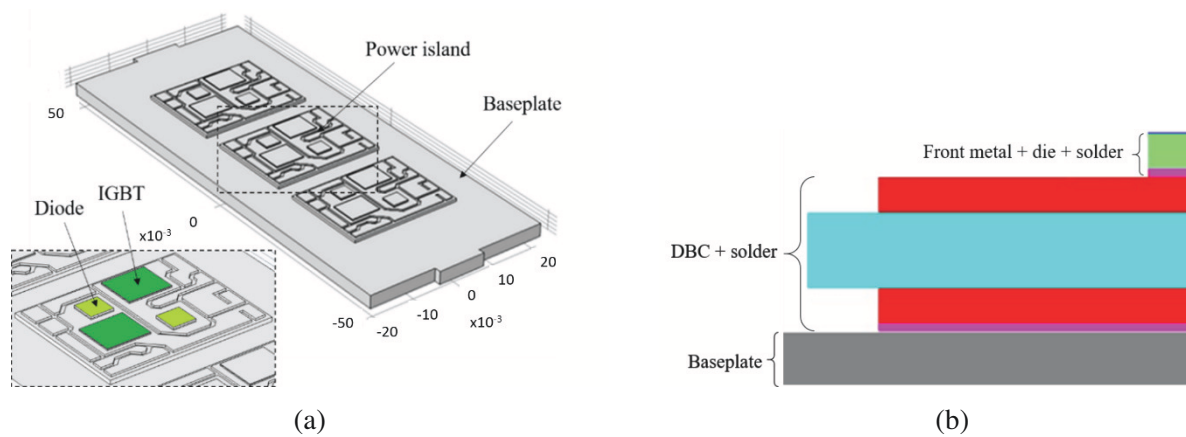


Figure 1. Geometry of the numerical model (a) and related stratigraphy (b). Baseplate is shown in grey, solders in magenta, DBC ceramic in cyan, DBC copper in red, dies in green and front metals in blue.

The physical properties of materials considered in our study are reported in Tab. 1.

Table 1. The physical properties of materials (ρ density, k thermal conductivity, C_p specific heat at constant pressure, α coefficient of volumetric thermal expansion, E Young's modulus, ν Poisson's ratio, σ_y Yield strength).

	ρ [kg/m ³]	k [W/(m·K)]	C_p [J/(kg·K)]	α [K ⁻¹]	E [MPa]	ν [-]	σ_y [MPa]
Copper	8900	360	393	1.6E-5	1.2E5	0.34	48
Solder (SnAgCu)	7370	75	220	2.2E-5	5.0E4	0.36	26
Ceramic	3260	150	734	4.5E-6	3.3E5	0.24	32
Silicon	2340	135	735	2.5E-6	1.8E5	0.22	40
Aluminium	2710	202	871	2.3E-5	7.0E4	0.33	11

2.2. Thermo-mechanical model

In the first step of our investigation, labelled from now Case A, a thermo-mechanical simulation was carried-out for the device, both in steady and transient conditions. It consisted in solving the following governing equations:

$$\rho C_p \frac{\partial T}{\partial t} = \nabla \cdot (k \nabla T) + Q \quad (1)$$

$$\sigma - \sigma_0 = C : (\varepsilon - \varepsilon_0 - \alpha \theta) \quad (2)$$

Eq. (1) represents the energy equation, where T is the temperature and Q is the volumetric heat generation. Eq. (2) is the Hooke's law relating the stress-strain of material, where σ is the stress tensor, σ_0 and ε_0 are initial stress and strain, C is the fourth order elasticity tensor, “:” stands for the double-dot tensor product and ε represents the total strain tensor, defined as:

$$\varepsilon = \frac{1}{2} (\nabla s + (\nabla s)^T) \quad (3)$$

where s is the displacement. Other symbols in eqns. (1) and (2) are referred to the caption of Tab. 1. Eqns. (2) and (3) were solved in order to detect the stress-strain thermally induced on the constitutive materials. The term θ appearing in eq. (2) denotes the difference between the local temperature T and the strain reference one T_{ref} , that corresponds to the baseplate temperature. This analysis was performed considering the worst working conditions in order to compute the maximum temperature and related stress-strain during the module functioning. To this goal, the bottom surface of the baseplate was held at constant temperature T_{ref} and a volumetric heat source was applied to all devices. Values of thermal heat sources correspond to the maximum power supplied to the devices during the module functioning. On all other boundaries, an insulation condition was applied. From the mechanical point of view, a fixed constraint was chosen for the bottom baseplate surface, maintaining free all other boundaries of the model. The structural load was related to the thermal computed state only.

2.3. Thermal fatigue model

In a second step of our investigation, labelled as Case B, a thermal fatigue life prediction was carried-out for the module. The target of this analysis was to assess the fatigue life of solder joints subjected to thermal cycles. The model proposed for predicting the fatigue life of solder layers is plastic strain based. As usually done when applying a plastic strain approach, time-independent plastic strain conditions are applied and the resulting stresses within a component are analysed.

2.3.1. Thermal cycle test

The computational model was built considering a thermal cycle between two environmental fixed temperatures. To this goal, and differently from what previously described for model implementation, we solved the energy equation in “passive” conditions. That means we applied different external conditions as thermal load to the device. In particular, no internal heat source was considered, while we applied two different thermal states ($T_c = -40$ °C and $T_h = 125$ °C) to the entire device external boundaries. This procedure simulates the module standing inside a climatic test room, held at two different constant control temperatures (cold temperature, T_c , and hot temperature, T_h). By means of this approach, the plastic strain range, $\Delta \varepsilon_p$, was evaluated by using the achieved thermal states. The ε_p is defined as the effective plastic strain, computed as a component of the total strain.

Then, in analogy to the Basquin equation, we applied the Coffin-Manson equation [5] to compute the number of cycles to failure, reading as follows:

$$\frac{\Delta \varepsilon_p}{2} = \varepsilon_f' (2N_f)^c \quad (4)$$

where ε'_f is the fatigue ductility coefficient and c is the fatigue ductility exponent of the solder material and finally N_f is the number of cycles to failure.

3. Numerical solution

Continuous equations were spatially discretized by a Finite Element approach based on the Galerkin method on non-uniform and non-structured computational grids made of tetrahedral Lagrange elements of order 2. Influence of spatial discretization was preliminary studied in order to assure mesh-independent results. A computational grid made of about 1230500 elements was retained for computations, giving 7835500 degrees of freedom. This mesh determines a maximum relative error of 4% with respect to the finer grid used for the preliminary mesh test made for this analysis. A snapshot of the used mesh is presented in Fig. 2. Steady solutions of discretized equations were carried-out by applying an iterative damped Newton-Raphson scheme [6], classically based on the discretized PDE linearization by a first-order Taylor expansion. Algebraic systems of equations coming from differential operators discretization have been solved by an Unsymmetrical Multi-Frontal package, a direct solver particularly efficient in order to solve unsymmetrical sparse matrixes by a LU decomposition method. For time-marching simulations we adopted an Implicit Differential-Algebraic (IDA) solver based on a variable-order and variable-step-size Backward Differentiation Formulas (BDF) [6]. Computations were carried-out on computational node made of 2 x 64 bit quad-core processors speeding up to 3.3 GHz of frequency and handling 512 GB of RAM.

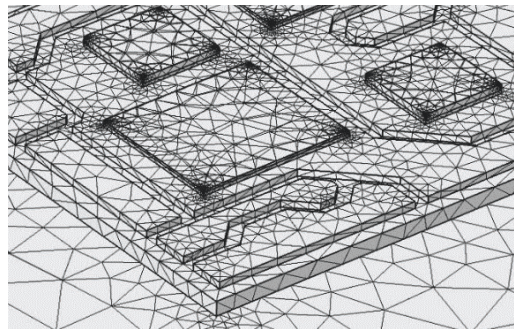


Figure 2. Mesh of the numerical model.

4. Results

Results were carried-out for different geometrical and constitutive configurations of the power module. In particular, different layer thickness were investigated and different physical properties were considered in solving the governing equations. In the following we present an extract of those results.

4.1. Thermo-mechanical analysis results

The thermal distribution obtained for a steady simulation of the module, when all devices are switched on and the maximum power (50 W for each IGBT and 10 W for each diode) is supplied through chips front metals, is shown in Fig. 3a (left side). In the enlargement of the picture, we report the maximum junction temperature value ($T_{jc}(\text{MAX}) = 41.6\text{ }^{\circ}\text{C}$) detected by simulation on the front metal of IGBT. The von Mises stress distribution, caused by the thermal load in Case A configuration, is shown in Fig. 3b (right side). The maximum value of von Mises stress computed for each module layer was compared to the ultimate strength of the constitutive materials. From comparison, tensile resistance results widely verified in spite of the worst thermal case considered.

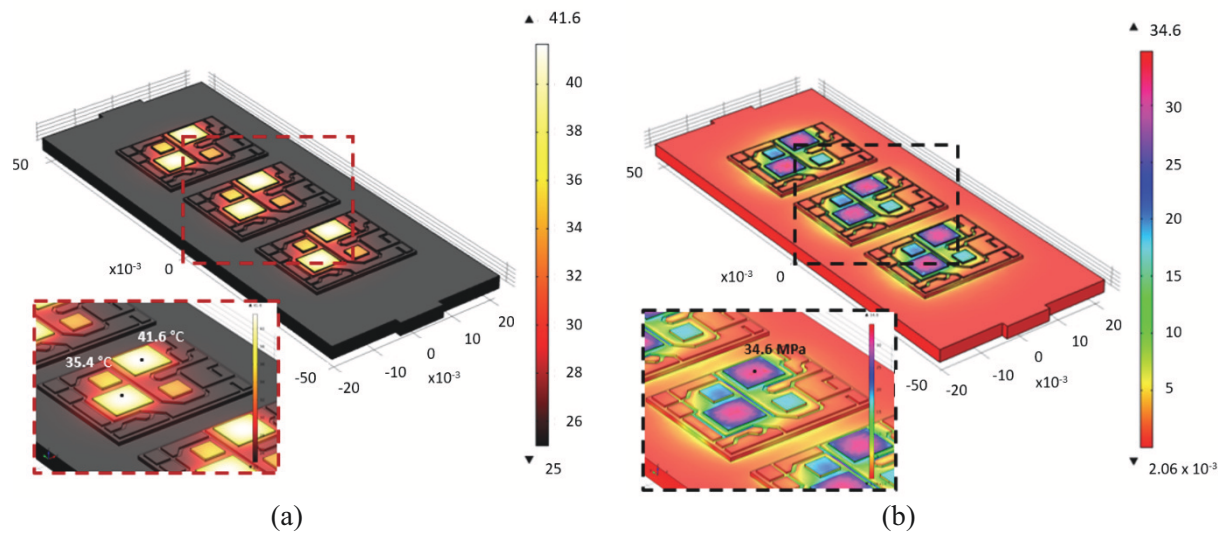


Figure 3. Thermal map [°C] (a) and stress distribution [MPa] (b) on the device and enlargements close to the central power island (Case A).

4.2. Thermal cycle test analysis results

Thermal states computed in Case B configuration were exploited for estimating the effective plastic strain distribution. The maximum value of ε_p was detected on the solder layer, joining the baseplate and the packed DBC. In particular, the most critical value of the effective plastic strain was detected in correspondence of the solder DBC corners. This is maybe due to the geometrical singularity.

Fig. 4a (left side) shows the effective plastic strain distribution in proximity of one of the solder DBC corner, where the highest value of ε_p was found in both environmental thermal conditions (T_c and T_h). This result well agrees with experimental evidences obtained by experimental activities developed on the power module. Fig. 4b (right side) shows two front-views of the module taken by a Scanning Acoustic Microscope (SAM). Pictures were taken at different time instants during a “thermal cycle” testing activity on the module. Environmental conditions applied in the climatic rooms during the experimental tests correspond to thermal levels used in computations. From experimental data reported in Fig. 4b it is possible to observe the damage produced on the module by the cyclic thermal load, in particular on the DBC solder. White regions (highlighted by the red arrows in the Fig. 4b) represent portions of the module where contact between layers fails. As attended, those regions were found in correspondence of the solder DBC corners. This establishment well agrees with some other findings of literature [7, 8].

As previously mentioned, from plastic strain evaluation it is possible to numerically assess the potential number of cycles to failure. In consequence, we were able to estimate the expected number of cycles to failure for SnAgCu solder layers, that are well-known the weakest part of the module from this point of view. From our investigation, the fatigue life prediction is approximately 1632 cycles for the solder die and 383 cycles for the solder DBC. Those results are in agreement with experimental evidences (solder DBC damaged between 300 and 600 cycles, solder die damaged after 1100 cycles). Successively a comparison study between SnAgCu and SnPb solder joints fatigue life was performed. From results, the fatigue life prediction for SnPb solder die is approximately 162672 cycles and 3071 for solder DBC. Those results well agree with evidences in literature showing that the fatigue life of SnAgCu solders is considerably lower than that of SnPb solder layers [9]. Experimental results that have been found in ref. [9] in similar tests indicate that at high board level strains SnPb solder out performs SnAgCu solder; in particular, the characteristic life was 19500 cycles for SnPb solder and 7730 cycles for SnAgCu solder.

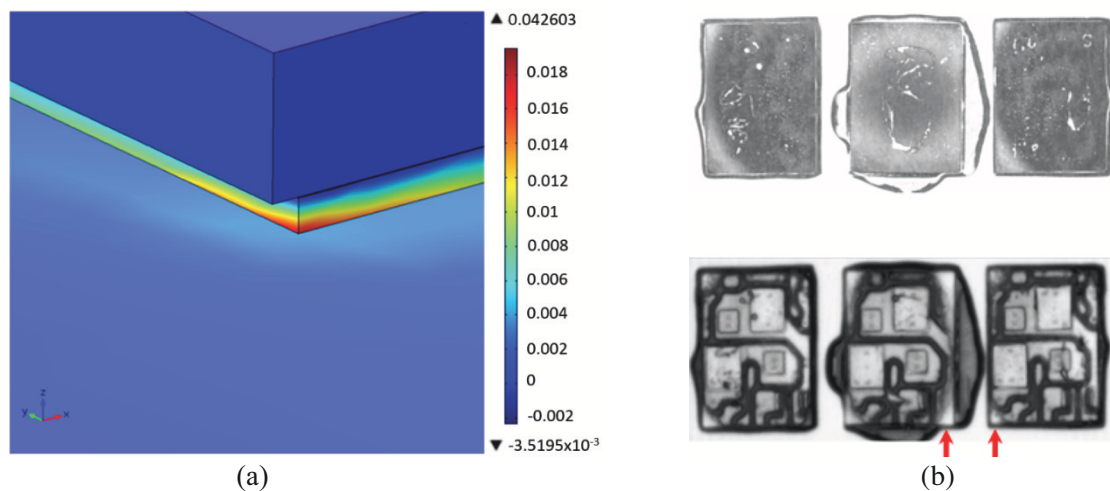


Figure 4. Effective plastic strain for one of the solder DBC corner, evaluated for $T_c=125\text{ }^{\circ}\text{C}$ (Case B) (a). SAM front-view of the module during a “thermal cycle” testing (b): pictures are reported for initial conditions (picture on top) and after 300 cycles (bottom picture). Red arrows indicate some detected damaged regions.

5. Conclusions

This work highlights the opportunity to exploit a numerical approach in order to simulate, from one hand, the thermo-mechanical behaviour of power module and, from another one, the fatigue life of module performing thermal cycles a two environmental fixed temperature inside a climatic test room. From results, it appears that thermal and thermo-mechanical levels are lower than potential critical values for constitutive materials, even in the worst working conditions. The fatigue life prediction results in good agreement with literature evidences and experimental findings. Module portions subjected by the highest plastic strain are regions closed to solder DBC corners. This is maybe due to the geometrical singularity. The fatigue life of SnAgCu solders is considerably lower than that of SnPb solders: for solder DBC it is one order of magnitude shorter, and two orders shorter for solder die.

References

- [1] Kim M and Yoon S W 2015 *Proc. EVS 28 (Goyang, Korea)*
- [2] Delmonte N, Giuliani F and Cova P 2013 *Microelectron. Rel.* **53** pp 1611-16
- [3] Sun Z, Benabou L and Dahoo P R *En. Fract. Mech.* **107** pp 48-60
- [4] Shinohara K and Yu Q 2011 *Int. J. Fatigue* **33** pp 1221-34
- [5] Manson S S 1966 (New York: McGraw-Hill)
- [6] Hindmarsh A C, Brown P N, Grant K E, Lee S L, Serban R, Shumaker D E and Woodward C S 2005 *ACM Trans. Math. Software* **31** pp 363-396
- [7] Mi J, Li Y F, Yang Y J, Peng W and Huang H Z 2014 *Sci. World J.* **1** pp 1-11
- [8] Lee W W, Nguyen L T and Selvaduray G S 2000 *Microelectron. Rel.* **40** pp 231-244
- [9] Blattau N and Hillman C 2005 *Proc. Int. Conf. on SMTA (Chicago, USA)*